Application of high-pressure homogenization to steer the technological functionalities of chia fibre-protein concentrate

APPLICATION OF HIGH-PRESSURE HOMOGENIZATION TO STEER THE TECHNOLOGICAL FUNCTIONALITIES OF CHIA FIBRE-PROTEIN CONCENTRATE

Niccolò Renoldi, Sofia Melchior, Sonia Calligaris, Donatella Peressini *

Department of Agricultural, Food, Environmental and Animal Sciences, University of Udine, Via Sondrio 2/A, 33100, Udine, Italy

* Corresponding author. E-mail: donatella.peressini@uniud.it (D. Peressini). Address: Department of Agricultural, Food, Environmental and Animal Sciences, University of Udine, Via Sondrio 2/A, Udine 33100, Italy

HIGHLIGHTS

- HPH triggered structural modifications and shaped functionalities of chia
- Insoluble fibre was partially converted in soluble fraction
- HPH promote new fibre-protein interactions leading to small aggregate formation
- 150-300 MJm^{-3} induced the best performing properties ensuring industrial feasibility
- HPH treated chia can be used in bakery product formulations high in dietary fibre

GRAPHICAL ABSTRACT

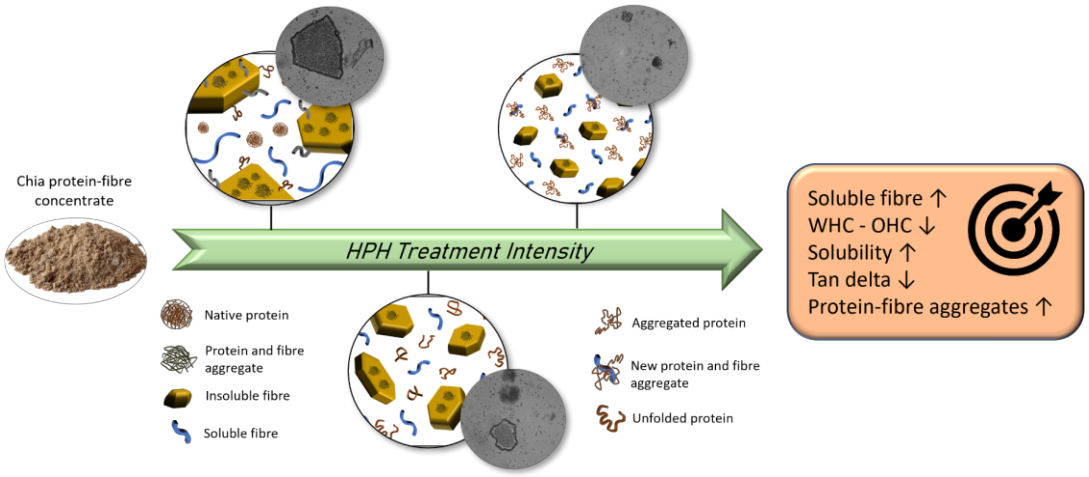

ABSTRACT

Chia is an excellent source of healthy constituents (dietary fibre and proteins) with high water holding capacity (WHC) and strong gelling properties, which imply technological challenges for its application in foods, such as leavened bakery products. Therefore, this work explored the potential of high-pressure homogenization (HPH) to steer the technological functionalities (physicochemical, structural and rheological properties) of a chia fibre-protein concentrate (FPC) for food applications. Chia FPC suspensions (5%, w/w) were treated at increasing pressures (up to 150 MPa) and number of cycles (up to 5) to generate a wide range of energy densities delivered to the sample during processing (100-750 MJ m^{-3}). HPH treatments decreased particle size, WHC and oil holding capacity of FPC. WHC of treated samples was 52-70% lower than control. Moreover, rheological measurements on the soluble fraction of homogenized FPC showed a reduction in apparent viscosity and shear-thinning behaviour. These results can be attributed to multiple events occurring during HPH processing. In particular, the mechanical forces suffered by the samples induced the rupture of native structures in smaller fragments in concomitance with biopolymer structure modifications. HPH at energy densities between 300 and 750 MJ m^{-3} determined a 14-35% increase in soluble dietary fibre (SDF) compared to control, indicating a partial conversion from insoluble to SDF without changes in total dietary fibre. Conformational changes in proteins were also observed. This study suggests that proper selection of HPH energy density represents a strategy to obtain novel promising ingredients rich in dietary fibre and proteins with tailored technological functionalities.

Keywords: mucilage, functional properties, water holding capacity, rheology, homogenizer, unfolding

1. Introduction

Seeds from *Salvia hispanica* L., also known as chia seeds, have been widely recognized as a potential source of nutrients with healthy properties, increasing their popularity (Alasalvar, Chang, Bolling, Oh, & Shahidi, 2021; Melo, MacHado, & Oliveira, 2019; Muñoz, Cobos, Diaz, & Aguilera, 2012). Besides being an excellent source of proteins, polyunsaturated fatty acids, and dietary fibre (Alasalvar et al., 2021; Melo et al., 2019; Sandoval-Oliveros & Paredes-López, 2013), chia seeds contain phenolic acids, especially quercetin and kaempferol, with potential antioxidant activity (Reyes-Caudillo, Tecante, & Valdivia-López, 2008). The main protein fractions are globulins (Sandoval-Oliveros & Paredes-López, 2013) and glutelins (Coelho & Salas-Mellado, 2018), which exhibit good thermal stability and technological functionalities including emulsifying, foaming, and gelling properties. Total dietary fibre (TDF) content in chia seeds varies from 20 to 40% (Alasalvar et al., 2021; Alfredo, Gabriel, Luis, & David, 2009; Melo et al., 2019; Reyes-Caudillo et al., 2008). Insoluble fibre (lignin, cellulose, and hemicellulose) represents 85% of TDF. The soluble fibre fraction mainly consists of a mucilaginous polysaccharide (gum) (Alfredo et al., 2009; Melo et al., 2019), which is structurally a linear repeating tetrasaccharide sequence composed of two D-xylopyranosyl residues, a D-glucopyranosyl unit, and side branches of 4-O-methyl-D-glucopyranosyluronic acid (Lin, Daniel, & Whistler, 1994). Besides, chia mucilage is rich in planteose, a trisaccharide belonging to the galactosyl-sucrose oligosaccharide group (Daudé, Remaud-Siméon, & André, 2012; Xing et al., 2017).

Generally, chia flour is obtained from seeds after partial oil extraction, resulting in a fibre-protein rich ingredient, suitable to enhance the nutritional properties of several food products (Aranibar et al., 2018; Mas et al., 2020; Zettel & Hitzmann, 2018). However,

66 incorporation of this ingredient in a food formulation could have detrimental effects on
67 the technological quality. This is especially the case of bakery products, in which chia
68 flour addition is expected to lower specific volume and increase crumb firmness of
69 leavened cereal-based products (Coelho & Salas-Mellado, 2015; Guiotto, Tomas, &
70 Haros, 2020; Steffolani, Martinez, León, & Gómez, 2015).
71 Application of non-thermal technologies could represent a promising strategy to modulate
72 the techno-functionalities of food biopolymers comprising those constituting chia
73 concentrate (Fayaz, Soleimanian, Mhamadi, Turgeon, & Khalloufi, 2022). Among all,
74 high-pressure homogenization (HPH) is under the spotlight due to its demonstrated ability
75 to promote structural changes of biopolymers, such as protein and carbohydrates (He,
76 2022; Saricaoglu, 2020). HPH is a dynamic pressure technology operating up to 400 MPa.
77 During processing the fluid product is subjected to high cavitation, elongational flow and
78 mechanical stresses (Floury, Bellettre, Legrand, & Desrumaux, 2004; Kubo, Augusto, &
79 Cristianini, 2013). Previous studies on HPH-treated soybean by-products and mustard
80 bran reported particle size reduction and increase in fibre interfacial area promoting a
81 more structured network (Colletti, Delgado, Cabezas, Wagner, & Porfiri, 2020; Donsì &
82 Velikov, 2020), as well as improvement in protein extraction yield from the matrix (Donsì
83 & Velikov, 2020; Fayaz, Plazzotta, Calligaris, Manzocco, & Nicoli, 2019; Plazzotta,
84 Moretton, Calligaris, & Manzocco, 2021). Investigations on HPH-treated sugar beet fibre
85 (Huang, Yang, Liu, & He, 2020) and citrus fibre (Su, Zhu, Wang, Li, & Wang, 2019)
86 showed increase in water and oil holding capacities due to conformational and structural
87 changes exhibiting new hydrophilic and/or hydrophobic regions. In addition, HPH
88 induced the conversion of around 8% insoluble fibre to soluble fraction in tomato residue
89 fibre (Hua et al., 2017) and soybean okara (Fayaz et al., 2019). Regarding the protein
90 fraction, HPH can be used to steer functional and interfacial properties by promoting

unfolding or aggregation phenomena as observed on faba bean (Yang, Liu, Zeng, & Chen, 2018), kidney bean (Guo et al., 2021) and lentil proteins (Saricaoglu, 2020).

To the best of our knowledge, there are no studies in the scientific literature on chia dispersions treated by HPH. Based on these considerations, this research aimed to investigate the impact of HPH treatment on physicochemical, structural, and rheological properties of a commercial chia fibre-protein concentrate by using different homogenization pressures (up to150 MPa) and number of passes (up to 5) to improve technological functionalities and thus industrial feasibility. In order to better evaluate the effects of HPH on specific components, analyses were carried out on the protein and dietary fibre fractions.

2. MATERIALS AND METHODS

2.1 Materials

A partially defatted chia fibre-protein concentrate (FPC) (56.0% dietary fibre, 24.7% protein, 9.0% fat, 4.7% ash and 4.7% moisture) was purchased from Benexia (Functional Products Trending S.A, Santiago, Chile). Commercial sunflower oil was used.

2.2 High-pressure homogenization of chia suspension

Chia FPC suspension (5%, w/w) was obtained by adding distilled water and magnetically stirring at room temperature for 24 h and 1,250 rpm. A continuous lab-scale high-pressure homogenizer (Panda Plus 2000, GEA Niro Soavi, Parma, Italy) equipped with two homogenization valves (flow rate of 10 L/h), was used to treat chia suspension (500 g). Working pressures of 0, 100 and 150 MPa for 1, 3 or 5 cycles were applied. Six different

116 treatments were carried out at homogenization energy densities from 0 to 750 MJ m^{-3}
117 (Table 1). The energy density was calculated as the pressure difference operating at the
118 nozzles according to Stang, Schuchmann, & Schubert (2001). The temperature of
119 homogenised samples was kept below 40 °C by cooling in ice-water bath after each pass.
120 After the treatment, samples were immediately blast chilled, frozen, and freeze-dried.
121 Freeze-dried samples (FDS) were used for further analyses. Experiments were performed
122 in duplicate, where each replicate corresponds to a separately chia suspension.
123

124 **2.3 Dietary fibre content**

125

126 Total dietary fibre (TDF), soluble dietary fibre (SDF), and insoluble dietary fibre (IDF)
127 contents of FDS were measured by using the total dietary fibre assay kit (Sigma Aldrich,
128 Milan, Italy) and following the enzymatic-gravimetric official method 985.29 (AOAC,
129 1997).
130

131 **2.4 Particle size distribution**

132

133 The particle size distribution of FDS was carried out by using a laser scattering particle
134 size distribution analyser (LA-950 Horiba, Kyoto, Japan). FDS were suspended in water
135 at room temperature and automatically kept in agitation for the analysis. The refractive
136 index was 1.47 and 1.33 for FDS and water, respectively. Distribution curves were
137 obtained from multiple measurements ($n > 3$).
138

2.5 Water and oil holding capacities

Distilled water or sunflower oil (1.5 g) was added to FDS (0.1 g), then the suspensions were mechanically stirred using a vortex (Vortex, Ika, Milan, Italy). After a stop of 15 min, the samples were centrifuged at 13,680×g for 10 min at 4 °C. The supernatant was removed, and the precipitate was weighed. The water (WHC, %) and oil holding capacities (OHC, %) were calculated by:

$$WHC\ or\ OHC = \frac{H - FDS}{FDS} * 100$$

where FDS is the weight (g on dry basis) of freeze-dried sample and H is the precipitate weight (g).

2.6 Powder and protein solubilities

The solubility of FDS was evaluated by suspending the samples in distilled water (1% w/w). The suspension was magnetically stirred for 4 h at room temperature, and centrifuged at 18,600×g for 15 min at 4 °C. The supernatant was collected, dried overnight at 70 °C in a vacuum oven (Vuotomatic 50, Bicasa, Milan, Italy), and weighed (Fs, g). Powder solubility (%) was measured by using the following equation (2):

$$Powder\ solubility\ (\%) = \frac{Fs}{FDS} * 100$$

where FDS is the weight (g on dry basis) of freeze-dried sample and Fs is the weight of the dried soluble fraction (g).

In order to evaluate protein solubility, FDS (1.75 g) was suspended in distilled water (5%, w/w), magnetically stirred for 1 h and centrifuged at 15,000×g for 20 min at 20 °C. Then, the supernatant was recovered and freeze-dried, while the insoluble pellet was discarded. Soluble protein content was evaluated through nitrogen Kjeldahl determination (N x 6.25) (Method 920.87, AOAC, 1997).

2.7 Absorbance at 280 nm

FDS (0.02 g) was suspended in 20 g of sodium phosphate buffer solution (0.05 M, pH 6.9) containing 0.5% SDS (w/v) (Sigma Aldrich, Milan, Italy). Suspension was magnetically stirred for 30 min at room temperature and centrifuged at 13,680×g for 10 min at 20 °C. The absorbance at 280 nm of the supernatant was measured at 25 °C by using a UV-Vis spectrophotometer (UV-2501 PC, Shimadzu Kyoto, Japan).

2.8 Determination of free SH groups

The concentration of total free sulfhydryl groups (SH) was determined according to the method of Panozzo et al. (2014) based on Ellman (1959) method. Briefly, chia samples (5 mg) were dispersed in 1.5 mL of 25% (w/v) SDS-Tris-Glycine-EDTA (SDS-TGE) buffer solution (pH 8) (Sigma Aldrich, Milan, Italy). Samples were mechanically stirred using a vortex, then added with 30 μL of Ellman's reagent (5′,5-di-thiobis (2-nitrobenzoic acid) or DTNB) (Sigma Aldrich, Milan, Italy) and incubated for 20 min at room

temperature. Samples were centrifuged at 16,000×g for 15 min at 4 °C. The supernatant was collected, and the absorbance was measured at 412 nm and 25 °C.

2.9 Surface hydrophobicity

Proteins surface hydrophobicity was tested by fluorescence analysis. The probe 1-anilino-8-naphthalene-sulfonate (ANS) was dispersed in the buffer solution (8 mM) and protected from the light. FDS (1 mg) was suspended in 1 mL of 0.1 M phosphate buffer solution (pH 7) for 1 h. Finally, samples were centrifuged for 10 min at 10,000×g and 4 °C. Supernatant (3 ml) was added with 18 μL of ANS solution and left reacting for 15 min in a dark place. Fluorescence intensity was measured using a fluorescence spectrophotometer (Cary Eclipse model, Agilent Technologies, Santa Clara, CA, USA). Samples were excited at 388 nm and the emission spectra was recorded from 400 to 700 nm.

2.10 Fourier transform infrared (FTIR) spectroscopy

FTIR spectra of FDS and freeze-dried soluble fractions (Fs) were acquired by an Alpha-P FTIR spectrometer (Bruker Optics, Milan, Italy) equipped with a diamond attenuated total reflection (ATR) Zn-Se crystal. Spectra were obtained over a wavelength range of 4000-400 cm^{-1} at 25 °C with a spectrum resolution of 4 cm^{-1}. Each collected spectrum was processed by using OPUS software (version 7.0, Bruker Optics, Milan, Italy) and Origin Pro 9 software (OriginLab, Northampton, MA, USA) according to Melchior, Calligaris, Bisson, & Manzocco (2020).

2.11 Optical microscopy

FDS suspensions (1%, w/w) were prepared adding distilled water and magnetically stirring for 4 h at room temperature, while chia mucilage was recovered and freeze-dried as described in section 2.6. An optical microscope (Leica DM2000, Leica Microsystems, Heerbrugg, Switzerland) with normal light was used to observe samples at 4× and 20× magnifications. A digital camera (Leica EC3) and the software Leica Suite LAS EZ (Leica Microsystem, Heerbrugg, Switzerland) were used to acquire and elaborate the images.

2.12 Fundamental rheology

Oscillatory and rotational shear tests were carried out using a controlled stress rheometer (Haake RheoStress 6000, Thermo Scientific, Karlsruhe, Germany).

FDS samples (1.3 g) were added with distilled water and gently mixed for 3 min using a spatula, to produce a dispersion with 68% (w/w) moisture content. To allow homogeneous hydration, FDS dispersion was rested at 25 °C for 20 min. Then, the sample was loaded between a parallel plate geometry (35 mm diameter and 2 mm gap) and rested additional 5 min before testing. To prevent drying, exposed surface was carefully coated with silicon oil. A frequency sweep test was conducted from 0.1 to 10 Hz at 25 °C and a stress amplitude below the limit of linear viscoelastic region (LVR). Storage modulus (G'), loss modulus (G") and loss tangent (tan δ = G"/G') vs. frequency were recorded and parameters at 1 Hz were used for statistical comparisons.

Besides, FDS (1.75 g) was suspended in distilled water (5%, w/w), magnetically stirred for 1 h and centrifuged at 15,000×g for 20 min at 20 °C. The sample separated into three

phases (from the top in the tube): a liquid phase (LP), a gel layer (GL) and insoluble particle phase. LP and GL were collected. Then, GL was gently dispersed in LP (3 min) giving a stable polymer solution for rheological testing using a concentric cylinder geometry (CC25 DIN Ti). Shear dependent behaviour under steady state conditions was evaluated at 25 °C by increasing shear rate from 3 to 100 s^{-1}. The sample was allowed to relax 5 minutes before analysis. The power law model was used to describe the relationship between shear stress (σ) and shear rate ($\dot{\gamma}$) according to equation (5):

$$\sigma = K\dot{\gamma}^n$$

where K is the consistency coefficient ($Pa \cdot s^n$) and n is the flow behaviour index (-).

For 100x3, 150x3 and 150x5 samples, Newton's equation was used to express the flow behaviour ($\sigma = \eta\,\dot{\gamma}$, where η is the viscosity coefficient).

2.13 Statistical analysis

Results were expressed as mean ± standard deviation of at least three measurements performed on two replicated experiments ($n \geq 3$). Bartlett's test was conducted to check the homogeneity of variance within all data groups. One-way analysis of variance (ANOVA) followed by Tukey's HSD test were used to determine statistically significant differences among means ($P < 0.05$) (R software, version 3.5.1, the R Foundation for Statistical Computing, Vienna, Austria).

3 Results and discussion

3.1 Effect of HPH on chia concentrate

The effect of HPH on particle size of chia flour is shown in Figs. 1 and 2. Particle size distribution of the control sample exhibited a main population with dimension around 200 μm along with a broad signal associated to the presence of smaller particles with variable dimensions (Fig. 1). An evident bimodal distribution was observed for HPH-treated samples at 100 MPa and 150 MPa for a single pass due to the increase in the number of smaller sized particles (around 22 μm), indicating a breakdown of large particles. The increase in the number of passes caused a shift to a monomodal distribution with a main peak at about 88 μm for homogenization at 150 MPa for 5 cycles. These results are attributable to the ability of HPH to cause fragmentation of particles due to the intense mechanical stress delivered by the process (Song, Zhou, Fu, Chen, & Wu, 2013; Yang et al., 2018). Previous works reported a decrease in particle size of soybean hull fibre at homogenization pressures of 30-100 MPa for 3 cycles (Colletti et al., 2020) and mustard bran treated at 150 MPa for 1-5 cycles (Donsì & Velikov, 2020).

Optical micrographs (Fig. 2) confirmed the ability of HPH to break down particles. Control (Fig. 2a) was characterized by the presence of big structures and aggregates of fibrous cell material, similar to those observed in mustard bran aqueous suspensions (Donsi et al., 2020). The increase in homogenization pressure and number of passes progressively induced the breakage of large particles to smaller size resulting in a more homogenous dispersion. These structural changes could affect functional properties of chia flour. To corroborate this hypothesis, solubility, water (WHC) and oil (OHC) holding capacities as well as rheological properties of chia suspensions were evaluated.

281 Homogenised samples showed significantly higher solubility ($P < 0.05$) than control
282 (Table 2). The 150x5 sample gave the greatest amount of the soluble fraction, probably
283 due to the highest HPH intensity. Earlier studies reported an increase in solubility of faba
284 bean proteins (Yang et al., 2018) and tomato fibre (Hua et al., 2017) after HPH treatment,
285 due to the formation of soluble aggregates and the conversion of insoluble to soluble fibre,
286 respectively.
287 WHC and OHC of control and treated samples are reported in Table 2. Both parameters
288 were significantly lower for HPH-treated samples compared to the control ($P < 0.05$).
289 Previous works on fibrous chia fractions (around 30% of TDF) identified soluble
290 mucilage and insoluble fibres (hemicellulose and lignin) as the major responsible of high
291 WHC values (Alfredo et al., 2009; Capitani, Spotorno, Nolasco, & Tomás, 2012).
292 Hydration properties of dietary fibres are strongly dependent on structural characteristics,
293 whereas oil absorption capacity is strictly related to surface properties of particles
294 (hydrophobicity and available area) (López et al., 1996). For specific applications such
295 as bakery products, DF-rich ingredients with reduced WHC are particularly interesting to
296 avoid competition for water between fibre and gluten proteins, which reflects on dough
297 development.
298 Rheological parameters from oscillatory test in LVR of treated chia dispersions are
299 reported in Table 2. The frequency sweep test of control and HPH-treated samples is
300 shown in Fig. 3. Storage modulus (G') data showed frequency dependence and tan δ
301 values below 1, indicating a weak gel behaviour for all samples. Control showed higher
302 storage modulus than HPH-treated samples. No significant differences in G' were
303 observed between 100x1, 150x1 and 100x3 suspensions, which gave lower values than
304 150x3 and 150x5 ($P = 0.05$). The shear modulus of a suspension depends on the volume
305 fraction of dispersed particles (ϕ). The equation of Eilers and Dijk established an increase

306 in shear modulus of a monodisperse suspension with ϕ, and introduced a limit of the solid
307 volume fraction or maximum packing fraction (ϕ_m) for concentrated suspensions (Ferry,
308 1980). The value of ϕ_m depends on particles size distribution, and it is higher for a
309 bidispersed suspension than monodispersed suspension, resulting in a lower shear
310 modulus (or relative viscosity) of the first one (He & Ekere, 2001). Thus, suspension
311 rheology can be influenced by varying the particle size distribution. Based on these
312 considerations and looking at rheological data of chia samples (Table 2), the decrease in
313 G' to a minimum for 100x1 and 150x1 could be attributed to change in particle size
314 distribution from monodisperse (control) to bimodal (Fig. 1). Moreover, it could not be
315 excluded that the treatment induced a modification of the groups exposed onto the particle
316 surface, thus affecting interparticle interactions. The rheological parameter tan δ was
317 significantly lower for HPH-treated samples than control (Table 2) ($P < 0.05$). Besides,
318 tan δ decreased with the increase in intensity of HPH treatment, which implied a more
319 solid-like behaviour probably due to the formation of clusters.
320 Based on the acquired results multiple mechanisms may explain the effect of HPH on
321 functional properties of chia concentrates: 1) breakage of the spongy structure of
322 insoluble fibre leading to partial shift to soluble fraction, as well as thinner and more open
323 structures (Chau, Wang, & Wen, 2007; Hua et al., 2017; Su et al., 2019); 2) re-
324 arrangements of protein conformations (Dissanayake & Vasiljevic, 2009) with an
325 increase in hydrophobic groups exposed on the surfaces (Guo et al., 2021; Yu et al.,
326 2018); 3) mechanical degradation of mucilaginous soluble fibre (Villay et al., 2012), and
327 consequently modification of its physicochemical properties (Coorey, Tjoe, & Jayasena,
328 2014; García-Salcedo, Torres-Vargas, del Real, Contreras-Jiménez, & Rodriguez-Garcia,
329 2018); 4) formation of new interactions between exposed residues of both proteins and

fibre polymers as a consequence of reduction in particle size and increase in surface area (Augusto, Ibarz, & Cristianini, 2012; Plazzotta et al., 2021).

3.2 Effect of HPH on protein fraction of chia flour

To understand the mechanisms behind changes in functional properties of HPH-treated chia flour, the protein fraction was deeply investigated. Soluble protein content was 27% (db) for the control. The amount of this fraction was significantly reduced by HPH treatments, but no significant differences were observed between treated samples ($P = 0.05$) (Table 3). It could be supposed that the HPH treatment probably induced conformational changes in proteins with the exposure of hydrophobic residues on the protein surface and/or the formation of insoluble aggregates responsible of the sharp reduction in WHC (Table 2) (Guo et al., 2021; Yu et al., 2018).

Although the increase in exposed aminoacidic hydrophobic groups in HPH-treated samples, OHC values slightly decreased (Table 2), indicating that proteins marginally influenced oil holding capacity. These results support the hypothesis that fibre fraction would mainly contribute to the increase in solubility of treated chia samples (Table 2).

Fourier transform infrared spectroscopy (FT-IR) was performed to assess variations in protein secondary structure. The Amide I region (1600-1700 cm^{-1}), which is related to the stretching vibrations of the C=O bonds of the amide groups, was analysed to predict modifications occurring in protein conformation (De Maria, Ferrari, & Maresca, 2016). Five main structures were detected corresponding to β-sheet intramolecular (~1613-1638 cm^{-1}), random coil (~1640-1648 cm^{-1}), α-helix (~1650 cm^{-1}), β-turn (~1670 cm^{-1}), and β-sheet intermolecular (~1690 cm^{-1}) (data not shown) (Carbonaro, Maselli, & Nucara, 2012; Carullo, Donsì, & Ferrari, 2020; Shevkani, Singh, Kaur, & Rana, 2015; Yang et al., 2018).

355 Table 3 shows the percentage accounted for secondary structures. HPH caused the
356 reduction in β-turns and the concomitant increase in random coil, whereas β-sheet firstly
357 decreased and then increased. Conversely, α-helix structure appeared more stable since
358 only slight variations were observed at 150 MPa for 3 cycles. In agreement with the
359 literature, results suggest that secondary structure of chia proteins is very susceptible to
360 HPH treatment due to changes in weak hydrogen bonds, which promote the
361 conformational transition of different secondary structures (Chen et al., 2019; Wu et al.,
362 2019; Yu et al., 2018).
363 Changes in protein tertiary and quaternary structure were evaluated by absorbance at 280
364 nm (A_{280}), extrinsic fluorescence and free -SH groups (Table 3; Fig. 4). Treated samples
365 showed A_{280} values significantly higher than control indicating the exposure of tyrosine
366 and tryptophan residues (Layne, 1957) ($P < 0.05$). The highest value was obtained at 100
367 MPa and 150 MPa for a single pass, while a pressure of 150 MPa for 5 cycles led to the
368 lowest value among treated samples. Based on these results, the increase in energy density
369 up a certain value of HPH treatment would reduce the exposure of tyrosine and tryptophan
370 residues.
371 The same trend was observed for extrinsic fluorescence, which is a measure of surface
372 hydrophobicity (Fig. 4). Homogenization at 150 MPa for a single pass gave maximum
373 fluorescence intensity indicating the exposition of hydrophobic groups that were
374 otherwise buried. The decrease in fluorescence intensity with the number of passes can
375 be considered the result of protein aggregation via hydrophobic interactions (Guo et al.,
376 2021; Yu et al., 2018; Zhao & Yang, 2009).
377 A progressive decrease in free thiol groups with HPH intensity was detected, suggesting
378 the formation of covalent disulphide bonds and other aggregation phenomena
379 (hydrophobic interactions) (Panozzo et al., 2014). HPH treatment could transfer excessive

energy to the matrix causing protein aggregation, which reduced exposure of free thiols (Maresca et al., 2017). Results suggest that HPH promoted the exposure of aromatic groups on the protein surface, while reassembling phenomena of extracted proteins occurred by increasing the number of cycles probably due to inter- and intramolecular interactions (Fayaz et al., 2019; Yu et al., 2018). Overall, obtained results showed that HPH energy density up to 150 MJ m^{-3} induced proteins unfolding, while further increase caused aggregation phenomena, as confirmed by other authors even if with different treatment magnitude (Carullo et al., 2020; Melchior, Moretton, Calligaris, Manzocco, & Nicoli, 2022).

3.3 Effect of HPH on fibre fraction of chia flour

Beside proteins, fibre fraction was also analysed to investigate the effect of HPH. Total dietary fibre (TDF), insoluble (IDF) and soluble (SDF) fibre contents were evaluated (Table 2). TDF of control was 64.5% (db). No significant differences in TDF were detected between control and treated samples ($P > 0.05$). However, HPH at 100 MPa for 3 cycles or 150 MPa for 3 and 5 cycles determined a 14-35% increase in SDF compared to control suggesting a partial conversion from IDF to SDF. Similar results were reported for other vegetable sources such as soybean okara and tomato fibre treated at 150 MPa for 5 cycles and 100 MPa for 10 cycles, respectively (Fayaz et al., 2019; Hua et al., 2017). Changes in SDF content are consistent with previous observations on particle size distribution (Fig. 1 and 2) and the hypothesized disruption at molecular level of the fibre structure, confirming the partial breakage of the original structure of IDF into smaller soluble fibre chains. These phenomena affected the chia flour functional properties leading to increase in solubility and decrease in WHC and OHC (Table 2). Acquired

405 results could be particularly important from a nutritional point of view since several
406 studies reported the beneficial effects of SDF, including antidiabetic properties and
407 reduction in cardiovascular diseases (Anderson et al., 2009; Brownlee, 2011).
408 After centrifugation and separation from the insoluble precipitate, the SDF fraction was
409 then analyzed separately to assess the effect of HPH treatment on soluble compounds.
410 Optical microscopy and FT-IR spectroscopy were used to evaluate mucilage freeze-dried
411 structure, the major component of SDF in chia seeds. Fig. 5 shows the images of control
412 and 150x5 sample. Control mucilage appeared as a compact network with scattered small
413 porous. This structure was previously defined as a combination of overlapping sheets by
414 Capitani, Ixtaina, Nolasco, & Tomás (2013). On the contrary, the treated sample showed
415 a less dense and organized structure, suggesting that HPH treatment induced physical
416 modification of soluble biopolymers by reducing the ability to form a network.
417 FT-IR analysis was used to further investigate structural differences between freeze-dried
418 soluble fractions. Fig. 6 shows FT-IR spectra for control and 150x5 sample. Evident
419 differences in structure of chia mucilage were detected between control and high pressure
420 treated sample by using infrared spectroscopy. HPH influenced the absorbance intensity
421 of typical chia mucilage bands. The first structural difference was detected on the band
422 between 3500 and 3100 cm^{-1} (peak at 3285 cm^{-1}), the region characterized by hydroxyl-
423 OH stretching in carbohydrates structures (Câmara et al., 2020). Three peaks, at 3012,
424 2923 and 2853 cm^{-1} which reflect -CH stretching modes typical of aromatic rings
425 (Timilsena, Adhikari, Kasapis, & Adhikari, 2016), were notably affected by the HPH
426 treatment. For the control sample a strong band appeared at 1743 cm^{-1} that represent the
427 C=O stretching vibration of the carboxyl group of uronic acid (Ren, Yakubov, Linter,
428 MacNaughtan, & Foster, 2020). In 150x5 sample spectra 1743 cm^{-1} peak almost
429 disappeared, probably suggesting the breakage of the sided branched 4-O-methyl-D-

430 glucopyranosyluronic acid from the mucilaginous tetrasaccharide linear structure. After
431 the amide region (1700 to 1600 cm^{-1}), the 1412 cm^{-1} peak relates to the symmetrical COO-
432 link stretching vibrations was found (Punia & Dhull, 2019). A weak band appeared at
433 1242 cm^{-1}, which is associate to the stretching of the C-O bond in carbohydrates (García-
434 Salcedo et al., 2018). At 1145 cm^{-1} a small peak was detected, corresponding to the
435 asymmetrical bending vibration of O-C-O group in pyranose ring (presence of
436 xyloglucan) (Punia & Dhull, 2019), while the intense 1034 cm^{-1} peak reflected the C-O-
437 C glycosidic bond stretching in sugar ring (Timilsena, Wang, Adhikari, & Adhikari,
438 2016).
439 Rheological measurements on the polymer solution resulting from liquid phase (LP) and
440 gel layer (GL), which were obtained by centrifugation, were conducted. The flow curves
441 (not shown) of polymer solutions showed a pseudoplastic behavior for control and treated
442 samples at 100 MPa and 150 MPa for a single pass (up to 150 MJ m^{-3}), whereas higher
443 energy densities gave Newtonian solutions (shear-independent behavior). Pseudoplastic
444 behavior was satisfactorily described by the power law model ($R = 0.998$-0.999), the
445 parameters of which are reported in Table 4. Control exhibited significantly higher
446 consistency coefficient (K) and lower flow index (n) than treated samples ($P < 0.05$),
447 mainly attributed to structural changes in SDF. HPH treatments seem to lower the
448 apparent viscosity (η_a) curve and the dependence of η_a from shear rate. In polymer
449 solutions, η_a is mainly controlled by how much the polymer chains interpenetrate. Higher
450 viscosity is associated with a greater number of entanglements between chains, which
451 make the flow more difficult. Results clearly indicated a partial SDF depolymerization of
452 SDF of HPH-treated samples, as previously found for other polysaccharides (Villay et
453 al., 2012), which affects the ability to form the mucilaginous network and to increase the
454 medium viscosity (Coorey et al., 2014; Ramos, Fradinho, Mata, & Raymundo, 2017).

Results have important implications for the bakery sector. Generally, the addition of high levels of DF to leavened cereal-based products, such as bread, cakes, and muffins, has detrimental effects on their volume expansion and crumb firmness (Elleuch et al., 2011). In fact, incorporation of DFs may weaken the gluten network or excessively increase dough/batter viscosity, leading to low expansion and undesired compact crumb. In this work, HPH was used to modify WHC and rheological properties of chia ingredient, making it more suitable to be incorporated in leavened starchy products. In addition, HPH promoted health benefits due to the increase in soluble dietary fibre.

Summarizing, Fig. 7 shows a schematic representation of the main structural and physicochemical changes in chia ingredient induced by HPH treatments. By increasing the HPH intensity, particles were progressively reduced (Figs. 1 and 2) due to the partial breakage of the original IDF structure leading to the formation of SDF (Table 2) which was probably characterized by smaller chains. Considering protein fraction, the treatment induces the exposure of free -SH and aminoacidic residues as well as hydrophobic groups on the protein surface, while the further increase in intensity induced protein unfolding (Table 3). Moreover, it could be supposed that HPH also induced the formation of new protein-fibre interactions, resulting in small clusters. Overall, the resulting functionalities of HPH treated chia samples might depends to the structural changes occurring to fibre fraction as well as to novel protein-fibre aggregates. In particular, the ability to hold water and oil as well as to form gel network was reduced while the solubility increased due to the resulting less dense structure (Fig. 3, Tables 2 and 4).

4 CONCLUSIONS

High-pressure homogenization technology at different processing conditions and energy density altered structural and physicochemical properties of chia products. Particle size, WHC, and OHC values were significantly reduced, probably due to the mechanical rupture of the fibre structures in smaller fragments and protein conformational changes. Solubility and SDF content results indicated a partial conversion of IDF to soluble polysaccharides. Furthermore, analysis on treated chia mucilage showed significant changes in FT-IR peak intensity and flow behaviours that may be caused by the depolymerization of soluble fibre with consequent inability to create networks. The protein fraction underwent structural changes, mainly due to the exposure of hydrophobic groups on the protein surface. The increase in number of passes induced reassembling phenomena of extracted proteins, probably due to hydrophobic interactions and formation of S-S bonds. In addition, structural modifications occurring to protein and fibre fractions might induce the formation of new smaller particles able to reassemble into new aggregates.

Overall, the HPH-structural modifications observed can be properly exploited shaping the techno-functionalities of chia dispersions at 150-300 MJ m^{-3}, which is compatible with the industrial feasibility. Moreover, these results open interesting horizons in DF rich food formulations. The HPH-driven properties of chia concentrate might be extremely important to produce leavened cereal products in which water availability and polymers interactions affects dough formation and handling, and the resulting textural properties.

In conclusion, further studies on the application of these HPH-treated chia powders in cereal-based products are recommended, to understand whether these functional ingredients could improve product technological and nutritional properties.

Author contribution

Niccolò Renoldi: Formal analysis; Data curation; Investigation; Writing - original draft; Visualization. **Sofia Melchior**: Formal analysis, Writing - review & editing - Supporting. **Sonia Calligaris**: Supervision; Conceptualization; Writing - review & editing. **Donatella Peressini**: Supervision; Conceptualization; Writing - review & editing - Lead.

Declaration of competing interest

None.

Funding

This research did not receive any specific grant from funding agencies in the public, commercial, or not-for profit sectors.

Ethical approval

Ethics approval was not required for this research.

Data availability statement

Data will be available on request.

5 REFERENCES

AOAC (1997). *Official methods of analysis of the Association of Official Analytical Chemists*, 16th ed. Gaithersburg, MD (USA): Association of Official Analytical Chemists.

Alasalvar, C., Chang, S. K., Bolling, B., Oh, W. Y., & Shahidi, F. (2021). Specialty seeds: Nutrients, bioactives, bioavailability, and health benefits: A comprehensive review. *Comprehensive Reviews in Food Science and Food Safety*, *20*, 2382–2427. https://doi.org/10.1111/1541-4337.12730

Alfredo, V. O., Gabriel, R. R., Luis, C. G., & David, B. A. (2009). Physicochemical properties of a fibrous fraction from chia (*Salvia hispanica* L.). *LWT - Food Science and Technology*, *42*, 168–173. https://doi.org/10.1016/j.lwt.2008.05.012

Anderson, J. W., Baird, P., Davis, R. H., Ferreri, S., Knudtson, M., Koraym, A., … Williams, C. L. (2009). Health benefits of dietary fiber. *Nutrition Reviews*, *67*, 188–205. https://doi.org/10.1111/j.1753-4887.2009.00189.x

Aranibar, C., Pigni, N. B., Martinez, M., Aguirre, A., Ribotta, P., Wunderlin, D., & Borneo, R. (2018). Utilization of a partially-deoiled chia flour to improve the nutritional and antioxidant properties of wheat pasta. *LWT - Food Science and Technology*, *89*, 381–387. https://doi.org/10.1016/j.lwt.2017.11.003

Augusto, P. E. D., Ibarz, A., & Cristianini, M. (2012). Effect of high pressure homogenization (HPH) on the rheological properties of tomato juice: Time-dependent and steady-state shear. *Journal of Food Engineering*, *111*, 570-579. https://doi.org/10.1016/j.jfoodeng.2012.03.015

Brownlee, I. A. (2011). The physiological roles of dietary fibre. *Food Hydrocolloids*, *25*, 238–250. https://doi.org/10.1016/j.foodhyd.2009.11.013

Câmara, A. K. F. I., Okuro, P. K., Cunha, R. L. da, Herrero, A. M., Ruiz-Capillas, C., & Pollonio, M. A. R. (2020). Chia (*Salvia hispanica* L.) mucilage as a new fat substitute in emulsified meat products: Technological, physicochemical, and rheological characterization. *LWT - Food Science and Technology*, *125*, Article 109193. https://doi.org/10.1016/j.lwt.2020.109193

Capitani, M. I., Ixtaina, V. Y., Nolasco, S. M., & Tomás, M. C. (2013). Microstructure, chemical composition and mucilage exudation of chia (*Salvia hispanica* L.) nutlets from Argentina. *Journal of the Science of Food and Agriculture*, *93*, 3856–3862. https://doi.org/10.1002/jsfa.6327

Capitani, M. I., Spotorno, V., Nolasco, S. M., & Tomás, M. C. (2012). Physicochemical and functional characterization of by-products from chia (*Salvia hispanica* L.) seeds of Argentina. *LWT - Food Science and Technology*, *45*, 94–102. https://doi.org/10.1016/j.lwt.2011.07.012

Carbonaro, M., Maselli, P., & Nucara, A. (2012). Relationship between digestibility and secondary structure of raw and thermally treated legume proteins: A Fourier transform infrared (FT-IR) spectroscopic study. *Amino Acids*, *43*, 911–921. https://doi.org/10.1007/s00726-011-1151-4

Carullo, D., Donsì, F., & Ferrari, G. (2020). Influence of high-pressure homogenization on structural properties and enzymatic hydrolysis of milk proteins. *LWT - Food Science and Technology*, *130*, Article 109657. https://doi.org/10.1016/j.lwt.2020.109657

Chau, C. F., Wang, Y. T., & Wen, Y. L. (2007). Different micronization methods significantly improve the functionality of carrot insoluble fibre. *Food Chemistry*, *100*, 1402–1408. https://doi.org/10.1016/j.foodchem.2005.11.034

Chen, H., Hong, Q., Zhong, J., Zhou, L., Liu, W., Luo, S., & Liu, C. (2019). The

enhancement of gastrointestinal digestibility of β-LG by dynamic high-pressure microfluidization to reduce its antigenicity. *International Journal of Food Science and Technology*, *54*, 1677–1683. https://doi.org/10.1111/ijfs.14044

Coelho, M. S., & Salas-Mellado, M. de las M. (2015). Effects of substituting chia (*Salvia hispanica* L.) flour or seeds for wheat flour on the quality of the bread. *LWT - Food Science and Technology*, *60*, 729–736. https://doi.org/10.1016/j.lwt.2014.10.033

Coelho, M. S., & Salas-Mellado, M. de las M. (2018). How extraction method affects the physicochemical and functional properties of chia proteins. *LWT - Food Science and Technology*, *96*, 26–33. https://doi.org/10.1016/j.lwt.2018.05.010

Colletti, A. C., Delgado, J. F., Cabezas, D. M., Wagner, J. R., & Porfiri, M. C. (2020). Soybean Hull Insoluble Polysaccharides: Improvements of its physicochemical properties through high pressure homogenization. *Food Biophysics*, *15*, 173–187. https://doi.org/10.1007/s11483-019-09613-y

Coorey, R., Tjoe, A., & Jayasena, V. (2014). Gelling Properties of Chia Seed and Flour. *Journal of Food Science*, *79*, Article E859–E866. https://doi.org/10.1111/1750-3841.12444

Daudé, D., Remaud-Siméon, M., & André, I. (2012). Sucrose analogs: An attractive (bio)source for glycodiversification. *Natural Product Reports*, *29*, 945–960. https://doi.org/10.1039/c2np20054f

De Maria, S., Ferrari, G., & Maresca, P. (2016). Effects of high hydrostatic pressure on the conformational structure and the functional properties of bovine serum albumin. *Innovative Food Science and Emerging Technologies*, *33*, 67–75. https://doi.org/10.1016/j.ifset.2015.11.025

Dissanayake, M., & Vasiljevic, T. (2009). Functional properties of whey proteins affected by heat treatment and hydrodynamic high-pressure shearing. *Journal of Dairy*

Science, *92*, 1387–1397. https://doi.org/10.3168/jds.2008-1791

Donsì, F., & Velikov, K. P. (2020). Mechanical cell disruption of mustard bran suspensions for improved dispersion properties and protein release. *Food and Function*, *11*, 6273–6284. https://doi.org/10.1039/d0fo00852d

Ellman, G. L. (1959). Tissue sulfhydryl groups. *Archives of Biochemistry and Biophysics*, *82*, 70–77. https://doi.org/doi.org/10.1016/0003-9861(59)90090-6

Fayaz, G., Plazzotta, S., Calligaris, S., Manzocco, L., & Nicoli, M. C. (2019). Impact of high pressure homogenization on physical properties, extraction yield and biopolymer structure of soybean okara. *LWT - Food Science and Technology*, *113*, Article 108324. https://doi.org/10.1016/j.lwt.2019.108324

Fayaz, G., Soleimanian, Y., Mhamadi, M., Turgeon, S. L., & Khalloufi, S. (2022). The applications of conventional and innovative mechanical technologies to tailor structural and functional features of dietary fibers from plant wastes: A review. *Comprehensive Reviews in Food Science and Food Safety*, *21*, 2149-2199. https://doi.org/10.1111/1541-4337.12934

Ferry, J. D. (1980). *Viscoelastic properties of polymers* (3rd ed.). John Wiley & Sons Inc. https://doi.org/10.1149/1.2428174

Floury, J., Bellettre, J., Legrand, J., & Desrumaux, A. (2004). Analysis of a new type of high pressure homogeniser. A study of the flow pattern. *Chemical Engineering Science*, *59*, 843–853. https://doi.org/10.1016/j.ces.2003.11.017

García-Salcedo, Á. J., Torres-Vargas, O. L., del Real, A., Contreras-Jiménez, B., & Rodriguez-Garcia, M. E. (2018). Pasting, viscoelastic, and physicochemical properties of chia (*Salvia hispanica* L.) flour and mucilage. *Food Structure*, *16*, 59–66. https://doi.org/10.1016/j.foostr.2018.03.004

Guiotto, E. N., Tomas, M. C., & Haros, C. M. (2020). Development of highly nutritional

625 breads with by-products of chia (*Salvia hispanica* L.) seeds. *Foods*, *9*, 1–13.
626 https://doi.org/10.3390/foods9060819
627 Guo, Z., Huang, Z., Guo, Y., Li, B., Yu, W., Zhou, L., … Wang, Z. (2021). Effects of
628 high-pressure homogenization on structural and emulsifying properties of thermally
629 soluble aggregated kidney bean (*Phaseolus vulgaris* L.) proteins. *Food*
630 *Hydrocolloids*, *119*, Article 106835. https://doi.org/10.1016/j.foodhyd.2021.106835
631 He, D., & Ekere, N. N. (2001). Viscosity of concentrated noncolloidal bidisperse
632 suspensions. *Rheologica Acta*, *40*, 591–598.
633 https://doi.org/10.1007/s003970100187
634 He, X., Dai, T., Sun, J., Liang, R., Liu, W., Chen, M., Chen, J., & Liu, C. (2022). Effective
635 change on rheology and structure properties of xanthan gum by industry-scale
636 microfluidization treatment. *Food Hydrocolloids*, *124*, Article 107319.
637 https://doi.org/10.1016/j.foodhyd.2021.107319
638 Hua, X., Xu, S., Wang, M., Chen, Y., Yang, H., & Yang, R. (2017). Effects of high-speed
639 homogenization and high-pressure homogenization on structure of tomato residue
640 fibers. *Food Chemistry*, *232*, 443–449.
641 https://doi.org/10.1016/j.foodchem.2017.04.003
642 Huang, X., Yang, Y., Liu, Q., & He, W. Q. (2020). Effect of high pressure
643 homogenization on sugar beet pulp: Physicochemical, thermal and structural
644 properties. *LWT - Food Science and Technology*, *134*, Article 110177.
645 https://doi.org/10.1016/j.lwt.2020.110177
646 Knorr, D., Froehling, A., Jaeger, H., Reineke, K., Schlueter, O., & Schoessler, K. (2011).
647 Emerging technologies in food processing. *Annual Review of Food Science and*
648 *Technology*, *2*, 203–235. https://doi.org/10.1146/annurev.food.102308.124129
649 Kubo, M. T. K., Augusto, P. E. D., & Cristianini, M. (2013). Effect of high pressure

650 homogenization (HPH) on the physical stability of tomato juice. *Food Research*
651 *International*, *51*, 170–179. https://doi.org/10.1016/j.foodres.2012.12.004
652 Lin, K. Y., Daniel, J. R., & Whistler, R. L. (1994). Structure of chia seed polysaccharide
653 exudate. *Carbohydrate Polymers*, *23*, 13–18. https://doi.org/10.1016/0144-
654 8617(94)90085-X
655 López, G., Ros, G., Rincón, F., Periago, M. J., Martínez, M. C., & Ortuño, J. (1996).
656 Relationship between Physical and Hydration Properties of Soluble and Insoluble
657 Fiber of Artichoke. *Journal of Agricultural and Food Chemistry*, *44*, 2773–2778.
658 https://doi.org/10.1021/jf9507699
659 Maresca, P., Ferrari, G., Júnior, B. R. de C. L., Zanphorlin, L. M., Ribeiro, L. R.,
660 Murakami, M. T., & Cristianini, M. (2017). Effect of dynamic high pressure on
661 functional and structural properties of bovine serum albumin. *Food Research*
662 *International*, *99*, 748–754. https://doi.org/10.1016/j.foodres.2017.06.047
663 Mas, A. L., Brigante, F. I., Salvucci, E., Pigni, N. B., Martinez, M. L., Ribotta, P., …
664 Baroni, M. V. (2020). Defatted chia flour as functional ingredient in sweet cookies.
665 How do Processing, simulated gastrointestinal digestion and colonic fermentation
666 affect its antioxidant properties? *Food Chemistry*, *316*, Article 126279.
667 https://doi.org/10.1016/j.foodchem.2020.126279
668 Melchior, S., Calligaris, S., Bisson, G., & Manzocco, L. (2020). Understanding the impact
669 of moderate-intensity pulsed electric fields (MIPEF) on structural and functional
670 characteristics of pea, rice and gluten concentrates. *Food and Bioprocess*
671 *Technology*, *13*, 2145–2155. https://doi.org/10.1007/s11947-020-02554-2
672 Melchior, S., Moretton, M., Calligaris, S., Manzocco, L., & Nicoli, M. C. (2022). High
673 pressure homogenization shapes the techno-functionalities and digestibility of pea
674 proteins. *Food and Bioproducts Processing*, *131*, 77–85.

https://doi.org/10.1016/j.fbp.2021.10.011

Melo, D., MacHado, T. B., & Oliveira, M. B. P. P. (2019). Chia seeds: an ancient grain trending in modern human diets. *Food and Function*, *10*, 3068–3089. https://doi.org/10.1039/c9fo00239a

Muñoz, L. A., Cobos, A., Diaz, O., & Aguilera, J. M. (2012). Chia seeds: Microstructure, mucilage extraction and hydration. *Journal of Food Engineering*, *108*, 216–224. https://doi.org/10.1016/j.jfoodeng.2011.06.037

Panozzo, A., Manzocco, L., Calligaris, S., Bartolomeoli, I., Maifreni, M., Lippe, G., & Nicoli, M. C. (2014). Effect of high pressure homogenisation on microbial inactivation, protein structure and functionality of egg white. *Food Research International*, *62*, 718–725. https://doi.org/10.1016/j.foodres.2014.04.051

Plazzotta, S., Moretton, M., Calligaris, S., & Manzocco, L. (2021). Physical, chemical, and techno-functional properties of soy okara powders obtained by high pressure homogenization and alkaline-acid recovery. *Food and Bioproducts Processing*, *128*, 95-101. https://doi.org/10.1016/j.fbp.2021.04.017

Punia, S., & Dhull, S. B. (2019). Chia seed (*Salvia hispanica* L.) mucilage (a heteropolysaccharide): Functional, thermal, rheological behaviour and its utilization. *International Journal of Biological Macromolecules*, *140*, 1084–1090. https://doi.org/10.1016/j.ijbiomac.2019.08.205

Ramos, S., Fradinho, P., Mata, P., & Raymundo, A. (2017). Assessing gelling properties of chia (*Salvia hispanica* L.) flour through rheological characterization. *Journal of the Science of Food and Agriculture*, *97*, 1753–1760. https://doi.org/10.1002/jsfa.7971

Ren, Y., Yakubov, G. E., Linter, B. R., MacNaughtan, W., & Foster, T. J. (2020). Temperature fractionation, physicochemical and rheological analysis of psyllium

seed husk heteroxylan. *Food Hydrocolloids*, *104*, Article 105737. https://doi.org/10.1016/j.foodhyd.2020.105737

Reyes-Caudillo, E., Tecante, A., & Valdivia-López, M. A. (2008). Dietary fibre content and antioxidant activity of phenolic compounds present in Mexican chia (*Salvia hispanica* L.) seeds. *Food Chemistry*, *107*, 656–663. https://doi.org/10.1016/j.foodchem.2007.08.062

Sandoval-Oliveros, M. R., & Paredes-López, O. (2013). Isolation and characterization of proteins from chia seeds (*Salvia hispanica* L.). *Journal of Agricultural and Food Chemistry*, *61*, 193–201. https://doi.org/10.1021/jf3034978

Sangnark, A., & Noomhorm, A. (2003). Effect of particle sizes on functional properties of dietary fibre prepared from sugarcane bagasse. *Food Chemistry*, *80*, 221–229. https://doi.org/10.1016/S0308-8146(02)00257-1

Saricaoglu, F. T. (2020). Application of high-pressure homogenization (HPH) to modify functional, structural and rheological properties of lentil (*Lens culinaris*) proteins. *International Journal of Biological Macromolecules*, *144*, 760–769. https://doi.org/10.1016/j.ijbiomac.2019.11.034

Shevkani, K., Singh, N., Kaur, A., & Rana, J. C. (2015). Structural and functional characterization of kidney bean and field pea protein isolates: A comparative study. *Food Hydrocolloids*, *43*, 679–689. https://doi.org/10.1016/j.foodhyd.2014.07.024

Song, X., Zhou, C., Fu, F., Chen, Z., & Wu, Q. (2013). Effect of high-pressure homogenization on particle size and film properties of soy protein isolate. *Industrial Crops and Products*, *43*, 538–544. https://doi.org/10.1016/j.indcrop.2012.08.005

Stang, M., Schuchmann, H., & Schubert, H. (2001). Emulsification in high-pressure homogenizers. *Engineering in Life Science*, *1*, 151–157. https://doi.org/10.1002/1618-2863(200110)1:4<151::AID-ELSC151>3.0.CO;2-D

725 Steffolani, E., Martinez, M. M., León, A. E., & Gómez, M. (2015). Effect of pre-hydration
726 of chia (*Salvia hispanica* L.), seeds and flour on the quality of wheat flour breads.
727 *LWT - Food Science and Technology*, *61*, 401–406.
728 https://doi.org/10.1016/j.lwt.2014.12.056
729 Su, D., Zhu, X., Wang, Y., Li, D., & Wang, L. (2019). Effects of high-pressure
730 homogenization on physical and thermal properties of citrus fiber. *LWT - Food*
731 *Science and Technology*, *116*, Article 108573.
732 https://doi.org/10.1016/j.lwt.2019.108573
733 Timilsena, Y. P., Adhikari, R., Kasapis, S., & Adhikari, B. (2016). Molecular and
734 functional characteristics of purified gum from Australian chia seeds. *Carbohydrate*
735 *Polymers*, *136*, 128–136. https://doi.org/10.1016/j.carbpol.2015.09.035
736 Timilsena, Y. P., Wang, B., Adhikari, R., & Adhikari, B. (2016). Preparation and
737 characterization of chia seed protein isolate-chia seed gum complex coacervates.
738 *Food Hydrocolloids*, *52*, 554–563. https://doi.org/10.1016/j.foodhyd.2015.07.033
739 Villay, A., de Filippis, F. L., Picton, L., Le Cerf, D., Vial, C., & Michaud, P. (2012).
740 Comparison of polysaccharide degradations by dynamic high-pressure
741 homogenization. *Food Hydrocolloids*, *27*, 278–286.
742 https://doi.org/10.1016/j.foodhyd.2011.10.003
743 Wu, F., Shi, X., Zou, H., Zhang, T., Dong, X., Zhu, R., & Yu, C. (2019). Effects of high-
744 pressure homogenization on physicochemical, rheological and emulsifying
745 properties of myofibrillar protein. *Journal of Food Engineering*, *263*, 272–279.
746 https://doi.org/10.1016/j.jfoodeng.2019.07.009
747 Xing, X., Hsieh, Y. S. Y., Yap, K., Ang, M. E., Lahnstein, J., Tucker, M. R., … Bulone,
748 V. (2017). Isolation and structural elucidation by 2D NMR of planteose, a major
749 oligosaccharide in the mucilage of chia (*Salvia hispanica* L.) seeds. *Carbohydrate*

Polymers, *175*, 231–240. https://doi.org/10.1016/j.carbpol.2017.07.059

Yang, J., Liu, G., Zeng, H., & Chen, L. (2018). Effects of high pressure homogenization on faba bean protein aggregation in relation to solubility and interfacial properties. *Food Hydrocolloids*, *83*, 275–286. https://doi.org/10.1016/j.foodhyd.2018.05.020

Yu, C., Wu, F., Cha, Y., Zou, H., Bao, J., Xu, R., & Du, M. (2018). Effects of high-pressure homogenization on functional properties and structure of mussel (*Mytilus edulis*) myofibrillar proteins. *International Journal of Biological Macromolecules*, *118*, 741–746. https://doi.org/10.1016/j.ijbiomac.2018.06.134

Zettel, V., & Hitzmann, B. (2018). Applications of chia (*Salvia hispanica* L.) in food products. *Trends in Food Science and Technology*, *80*, 43–50. https://doi.org/10.1016/j.tifs.2018.07.011

Zhao, W., & Yang, R. (2009). Effect of high-intensity pulsed electric fields on the activity, conformation and self-aggregation of pepsin. *Food Chemistry*, *114*, 777–781. https://doi.org/10.1016/j.foodchem.2008.10.016

CAPTIONS OF FIGURES

Fig. 1. Particle size distribution of HPH-treated chia samples.

Fig. 2. Micrographs of HPH-treated chia samples. Control (A_1, B_1), 100x1 (A_2, B_2), 150x1 (A_3, B_3), 100x3 (A_4, B_4), 150x3 (A_5, B_5) or 150x5 (A_6, B_6). Magnifications of 4x (A_1-A_6) and 20x (B_1-B_6).

Fig. 3. Storage (G', close symbol) and loss (G", open symbol) moduli as a function of frequency for HPH-treated chia dispersions at 68% moisture content and 25 °C. Control (circle), 150x1 (triangle) or 150x3 (square).

Fig. 4. ANS fluorescence spectra of HPH-treated chia samples.

Fig. 5. Micrographs of HPH-treated chia mucilage. Control (A_1, B_1) or 150x5 (A_2, B_2). Magnifications of 10x (A_1-A_2) and 20x (B_1-B_2).

Fig. 6. FT-IR spectra of soluble fraction for control and HPH-treated chia sample (150x5).

Fig. 7. Schematic representation of the main structural and physicochemical changes in chia ingredient induced by HPH treatments.

CAPTIONS OF TABLES

Table 1. Processing conditions (pressure and number of cycles) and energy density of HPH treatments.

Table 2. Physicochemical and rheological properties, and dietary fibre content of control and HPH-treated chia samples.

Table 3. Protein solubility, absorbance at 280 nm (A_{280}), free sulfhydryl (SH) groups, and FT-IR protein secondary structure of control and HPH-treated chia samples.

Table 4. Rheological parameters of the power law model and Newtonian viscosity (η) for soluble fraction of control and HPH-treated chia samples.

FIGURE 1

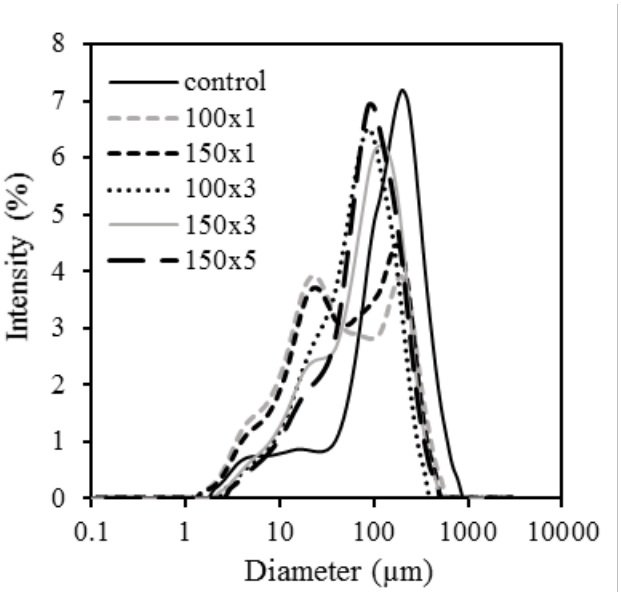

FIGURE 2

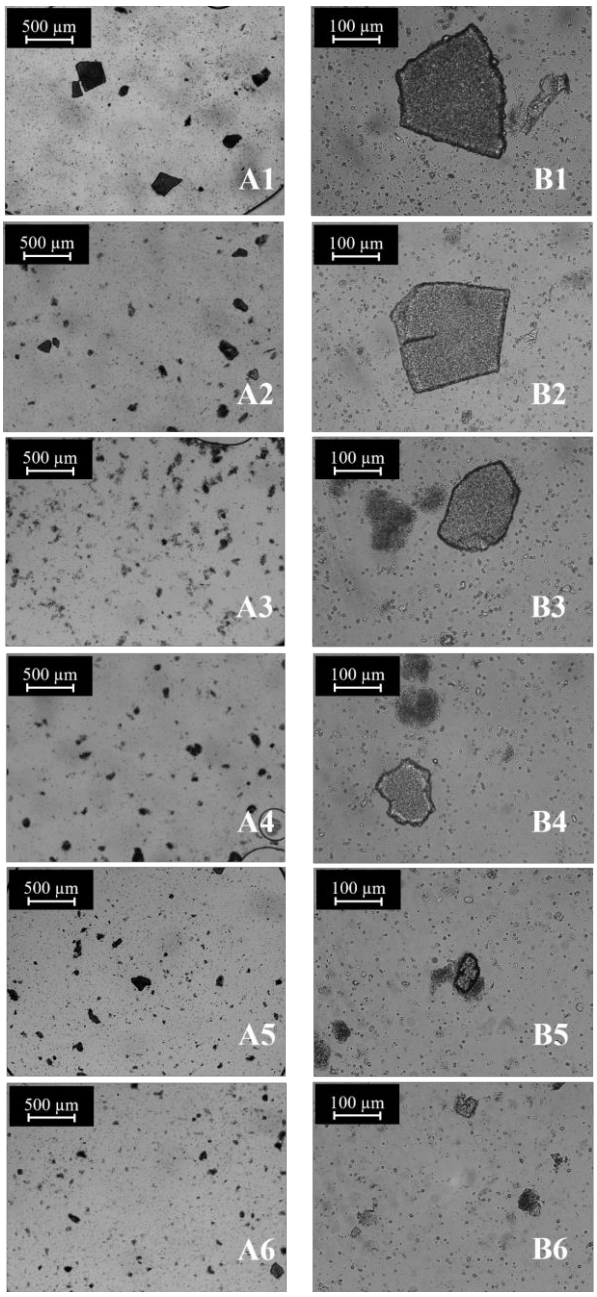

FIGURE 3

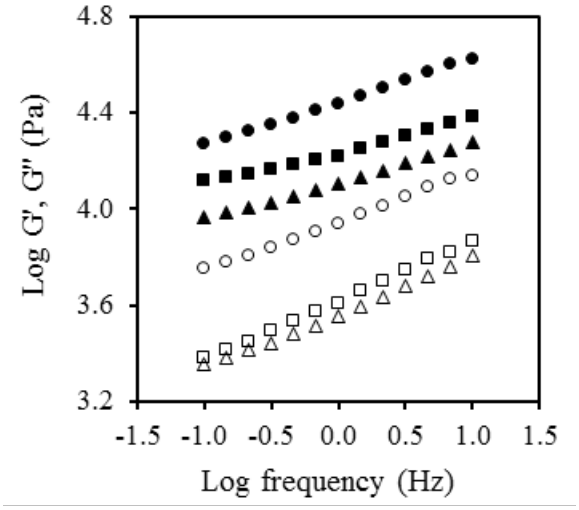

FIGURE 4

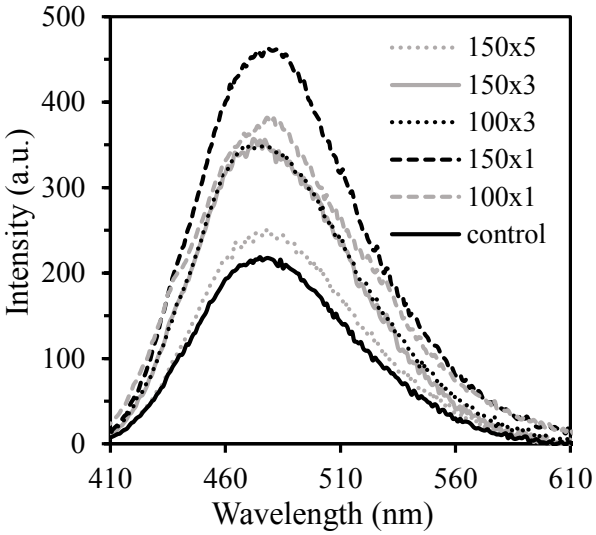

FIGURE 5

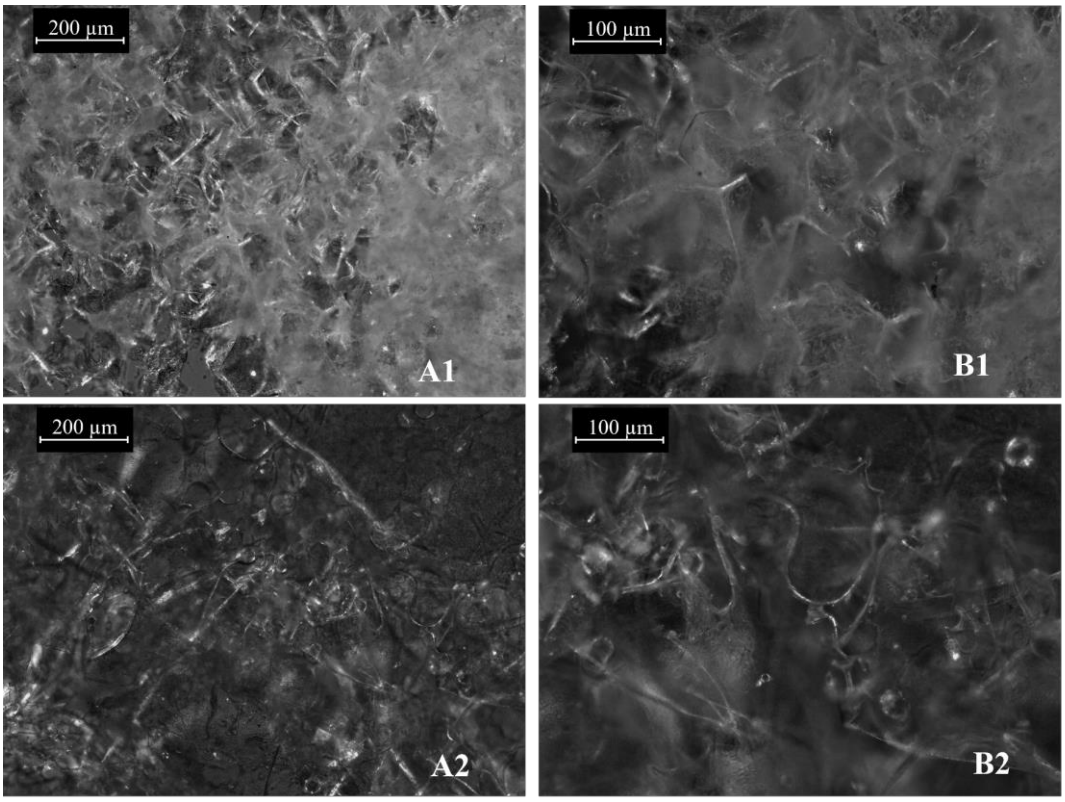

FIGURE 6

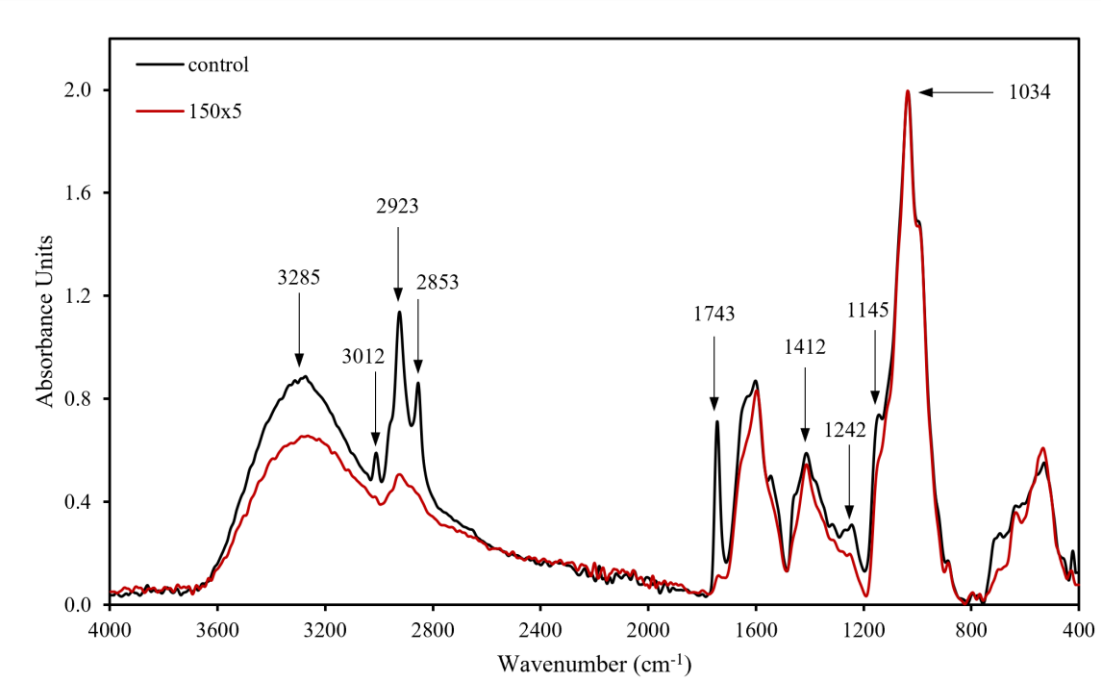

FIGURE 7

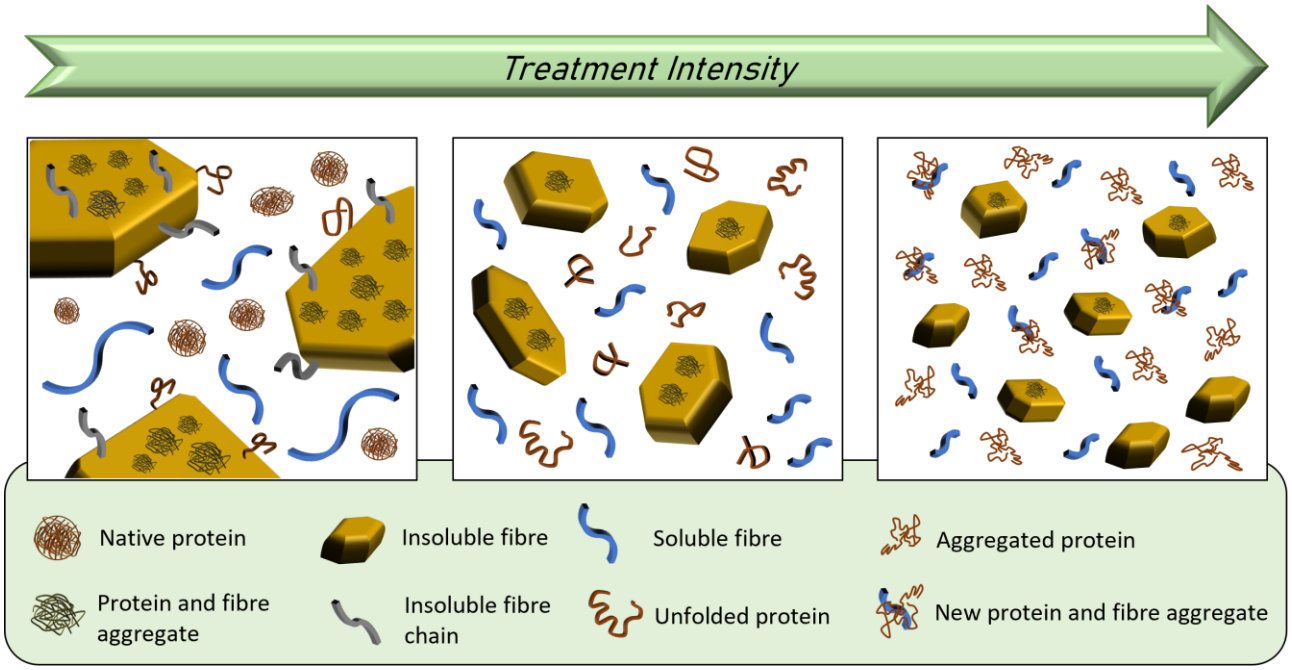

TABLE 1

Table 1. Processing conditions (pressure and number of cycles) and energy density of HPH treatments.

Samples	Pressure (MPa)	Cycles (n°)	Energy density (MJ m^{-3})
Control	0	1	0
100x1	100	1	100
150x1	150	1	150
100x3	100	3	300
150x3	150	3	450
150x5	150	5	750

TABLE 2

Table 2. Physicochemical and rheological properties, and dietary fibre content of control and HPH-treated chia samples.

Samples	Solubility (%)	WHC (%)	OHC (%)	G' (kPa)[a]	tan delta (-)[a]	TDF (% db)	IDF (% on TDF)	SDF (% on TDF)
Control	15.5 ± 0.3^{c}	546 ± 11^{a}	536 ± 6^{a}	27.2 ± 0.7^{a}	0.316 ± 0.003^{a}	64.49 ± 0.29^{a}	89.44 ± 0.45^{a}	10.56 ± 0.45^{c}
100x1	17.6 ± 0.3^{b}	261 ± 7^{b}	559 ± 7^{a}	13.1 ± 0.0^{d}	0.298 ± 0.004^{b}	64.87 ± 0.77^{a}	89.67 ± 0.02^{a}	10.33 ± 0.02^{c}
150x1	17.1 ± 0.5^{b}	180 ± 8^{cd}	478 ± 20^{b}	12.7 ± 0.3^{d}	0.283 ± 0.001^{c}	65.17 ± 0.90^{a}	89.02 ± 0.58^{ab}	10.98 ± 0.58^{bc}
100x3	16.9 ± 0.3^{b}	176 ± 3^{cd}	479 ± 16^{b}	12.4 ± 0.2^{d}	0.256 ± 0.002^{d}	65.84 ± 0.28^{a}	87.64 ± 0.10^{b}	12.36 ± 0.10^{b}
150x3	16.9 ± 0.3^{b}	164 ± 3^{d}	479 ± 9^{b}	16.6 ± 0.5^{c}	0.243 ± 0.005^{e}	65.72 ± 0.84^{a}	87.94 ± 0.15^{b}	12.06 ± 0.15^{b}
150x5	20.8 ± 0.3^{a}	187 ± 4^{c}	488 ± 9^{b}	23.0 ± 0.2^{b}	0.205 ± 0.002^{f}	66.17 ± 0.48^{a}	85.79 ± 0.55^{c}	14.21 ± 0.55^{a}

Mean ± standard deviation ($n \geq 3$). Values within a column followed by the same letter are not significantly different Tukey test ($P > 0.05$). db: dry basis. WHC: water holding capacity. OHC: oil holding capacity. TDF: total dietary fibre. IDF: insoluble dietary fibre. SDF: soluble dietary fibre.

[a] Values at 1 Hz obtained from the frequency sweep test at 25 °C on chia dispersions (68% moisture content).

TABLE 3

Table 3. Protein solubility, absorbance at 280 nm (A_{280}), free sulfhydryl (SH) groups, and FT-IR protein secondary structure of control and HPH-treated chia samples.

Samples	Soluble proteins (%)	A_{280} (-)	Free SH groups ($\mu M\ g^{-1}$)	Intermolecular β-sheet (%)[a]	Intramolecular β-sheet (%)[a]	Random coil (%)[a]	α-helix (%)[a]	β-turn (%)[a]
Control	27.6 ± 1.3^{a}	0.643 ± 0.003^{d}	73.8 ± 1.9^{a}	17.0 ± 0.7^{b}	25.9 ± 0.8^{a}	12.0 ± 1.0^{b}	24.1 ± 1.0^{a}	18.1 ± 0.6^{a}
100x1	19.8 ± 0.6^{b}	0.739 ± 0.003^{a}	70.5 ± 0.7^{a}	14.4 ± 0.9^{c}	21.3 ± 0.4^{c}	20.4 ± 0.8^{a}	23.8 ± 0.3^{a}	17.9 ± 0.3^{ab}
150x1	18.7 ± 0.3^{b}	0.749 ± 0.004^{a}	59.3 ± 0.5^{b}	15.4 ± 0.9^{bc}	23.2 ± 0.6^{b}	20.3 ± 0.6^{a}	24.0 ± 0.5^{a}	15.7 ± 0.7^{c}
100x3	18.3 ± 0.2^{b}	0.715 ± 0.003^{b}	56.9 ± 0.5^{c}	15.9 ± 1.1^{bc}	21.9 ± 0.8^{bc}	22.0 ± 0.8^{a}	24.7 ± 0.4^{a}	15.0 ± 1.0^{c}
150x3	17.9 ± 0.2^{b}	0.709 ± 0.004^{b}	46.5 ± 0.6^{d}	17.4 ± 0.9^{b}	18.9 ± 0.8^{d}	20.6 ± 1.4^{a}	18.8 ± 1.0^{b}	16.1 ± 0.6^{bc}
150x5	18.4 ± 0.5^{b}	0.691 ± 0.005^{c}	41.5 ± 0.4^{e}	23.0 ± 1.0^{a}	22.4 ± 0.5^{bc}	20.4 ± 0.2^{a}	24.7 ± 0.2^{a}	11.9 ± 0.9^{d}

Mean ± standard deviation ($n \geq 3$). Values within a column followed by the same letter are not significantly different Tukey test ($P > 0.05$).

[a] Protein amide I region obtained from FT-IR analysis.

TABLE 4

Table 4. Rheological parameters of the power law model (K and n) and Newtonian viscosity (η) for soluble fraction of control and HPH-treated chia samples.

Samples	η (mPa s)	K (mPa s^n)	n (-)	R^2
Control	-	146.5 ± 18.7^{a}	0.605 ± 0.025^{d}	0.999
100x1	-	7.0 ± 0.4^{b}	0.903 ± 0.014^{c}	0.998
150x1	-	5.4 ± 0.5^{b}	0.939 ± 0.013^{bc}	0.999
100x3	2.7 ± 0.2^{a}	-	-	0.999
150x3	2.3 ± 0.1^{a}	-	-	1.000
150x5	1.8 ± 0.0^{b}	-	-	1.000

Mean ± standard deviation ($n \geq 3$). Values within a column followed by the same letter are not significantly different Tukey test ($P > 0.05$).
n: flow behavior index. K: consistency coefficient.